Available online at www.sciencedirect.com

SciVerse ScienceDirect

Ceramics International 39 (2013) 1717–1722

CERAMICS INTERNATIONAL

www.elsevier.com/locate/ceramint

Phase evolution and reduction behavior of $Ce_{0.6}Zr_{0.4}O_2$ powders prepared using the chemical co-precipitation method

Chia-Che Chuang[a], Hsing-I Hsiang[a,*], Fu-Su Yen[a], Chih-Cheng Chen[b], Shien-JenYang[c]

[a]*Particulate Materials Research Center, Department of Resources Engineering, National Cheng Kung University, No.1, University Road, Tainan 70101, Taiwan*

[b]*Department of Mechanical Engineering, Far East University, No.49, Jhonghua Road, Shinshih Township, Tainan 744, Taiwan*

[c]*Department of Materials Science and Engineering, Far East University, No.49, Jhonghua Road, Shinshih Township, Tainan 744, Taiwan*

Received 17 May 2012; received in revised form 3 August 2012; accepted 9 August 2012
Available online 18 August 2012

Abstract

The relationship between the crystalline structure and reduction behavior of $Ce_{0.6}Zr_{0.4}O_2$ (C60Z) synthesized using the chemical co-precipitation method is investigated. C60Z decomposes into Ce-rich and Zr-rich phases after calcination at above 1100 °C for 2 h. The phase separation deteriorates the reducibility and oxygen storage capacity, indicating that reduction behavior is degraded by chemical inhomogeneity due to phase separation. The two separated phases transform into pyrochlore after heat treatment at 1490 °C under a 5% CO/N_2 atmosphere and then transform back into the separated phases after subsequent heat treatment in air. These results suggest that the structural change under reduction/re-oxidation treatment may result from cation diffusion.

Keywords: Cold-start emission; Oxygen storage capacity; Phase separation; Pyrochlore

1. Introduction

CeO_2 is widely used as a promoter for automotive exhaust catalysts due to its unique oxygen storage/release property (i.e., oxygen storage capacity, OSC) under an oxidizing/reducing atmosphere [1–3]. However, the thermal stability and OSC of pure ceria are degraded after high temperature treatment [3–5]. With increased demand for cleaner exhaust gases, catalysts are required to improve the oxygen release properties, especially for cold-start emission applications [1,6,7]. The reducibility of ceria is greatly enhanced when it is mixed with zirconia to form a solid solution of $Ce_xZr_{1-x}O_2$ (CZ, $1 > x > 0$) [8,9]. There are many explanations for the improved reduction behavior of CZ, including facilitating oxygen defects [3,8], higher oxygen mobility (i.e., lower oxygen migration energy) [1,5,9], and longer cation–oxygen bond length (i.e., lower cation–oxygen binding energy) [10,11]. For the CZ system, the optimal OSC has been obtained for $Ce_xZr_{1-x}O_2$ with $0.6 \le x \le 0.8$ [9,12,13]. However, the origin of the improved redox property due to ZrO_2 doping has not yet been fully resolved [4].

The typical reduction behavior of CZ systems can be divided into those in the low- and high-temperature regions. Some reports [2,14] have suggested that low-temperature reduction belongs to the surface reduction of the CZ system, which follows the reduction behavior of pure ceria [15,16]. However, other researchers have suggested that other easier reduction species might exist besides surface reduction at low temperature [3,9,16]. The reduction profiles were quite similar for samples with low and high surface areas in the CZ system [6,17,18], indicating that the reduction behavior might not be directly related to the specific surface area.

Another important aspect is the order–disorder phase transformation of CZ during reduction/oxidation treatment. After heat treatment at high temperature, the CZ structure transforms from a solid solution (disorder) into a pyrochlore (order) structure under a reducing atmosphere. The pyrochlore structure then returns back into a CZ solid

*Corresponding author. Tel.: +886 6 27527575x62821; fax: +886 6 2380421.
E-mail address: hsingi@mail.ncku.edu.tw (H.-I. Hsiang).

0272-8842/$ - see front matter © 2012 Elsevier Ltd and Techna Group S.r.l. All rights reserved.
http://dx.doi.org/10.1016/j.ceramint.2012.08.016

solution under an oxidation atmosphere [7,19–23]. The CZ phase transformation seems reversible during redox treatments. Many researchers have described the order–disorder phase transition phenomenon for CZ, but its transition mechanism is still unclear.

The present study investigates the relationship between the crystalline structure and the reduction behavior of $Ce_{0.6}Zr_{0.4}O_2$ powders and the phase transformation of $Ce_{0.6}Zr_{0.4}O_2$ after high temperature reduction/re-oxidation treatment.

2. Experimental procedure

$Ce_{0.6}Zr_{0.4}O_2$ (C60Z, molar ratio of Ce: Zr = 6:4) powder was synthesized using a chemical co-precipitation method. Briefly, stoichiometric amounts of ammonium cerium (IV) nitrate ($(NH_4)_2Ce(NO_3)_6$, J.T. Baker, >99%) and zirconium (IV) dinitrate oxide ($ZrO(NO_3)_2 \cdot 6H_2O$, Sigma-Aldrich, >99%) were dissolved in distilled water. The solutions were mixed and then slowly dripped into an aqueous NH_4OH solution. The pH value of the co-precipitating solution was maintained at 9 by adding a 10% NH_4OH solution. The obtained precipitate was filtered, washed using distilled water twice, and then with isopropanol twice to remove anion impurities. The mixture was then dried at 80 °C for 48 h. The obtained cakes were ground into powders and then calcined at various temperatures (700, 900, 1000, 1100, and 1200 °C) for 2 h (heating rate: 5 °C/min) in air.

Powder X-ray diffraction (XRD) data were collected using Siemens D5000 ($CuK_{\alpha 1}$ radiation, 40 kV, and 40 mA). The BET specific surface area was determined using a standard nitrogen adsorption–desorption technique (Micromeritics ASAP2020). The reducibility was characterized using thermogravimetric analysis (TGA; Netzsch STA409 PC) in a flow of 50 ml/min 5% CO/N_2 with heating to 1490 °C (rate: 10 °C/min) after the system was evacuated two times. The reduction/re-oxidation procedure was also characterized using TGA. After the system was evacuated two times, the reduction was carried out in a 20 ml/min 5% CO/N_2 flow from room temperature to 800 °C (rate: 5 °C/min), and held at this temperature for 1 h. Following the re-oxidation procedure in a flow of 20 ml/min 21% O_2/N_2 from 800 to 150 °C (rate: 5 °C/min), the reduction/re-oxidation sequence was performed for two cycles. The OSC value was measured using the weight gain under the oxidation step (800–150 °C, under 21% O_2/N_2 atmosphere) during the first cycle.

3. Results and discussion

Fig. 1 shows XRD patterns of the C60Z samples calcined at 700–1200 °C for 2 h. A single cubic phase of $Ce_{0.6}Zr_{0.4}O_2$ solid solution was observed when the calcination temperature was below 1000 °C. Compared to the XRD peaks of the samples calcined at 700–900 °C, those of the sample calcined at 1000 °C for 2 h were shifted

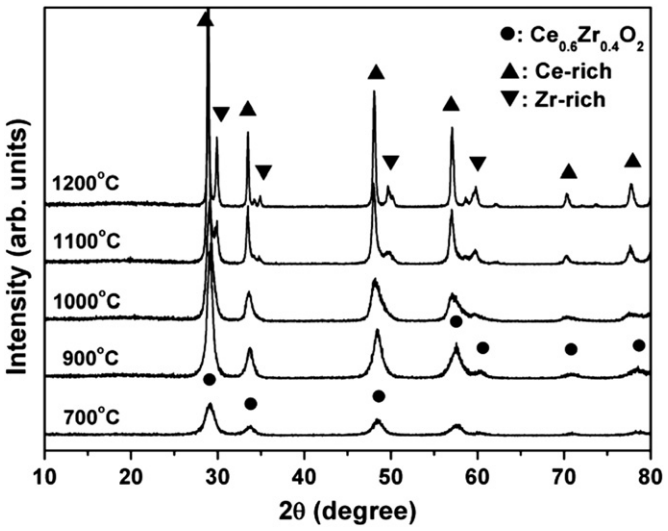

Fig. 1. XRD patterns of C60Z samples calcined at 700–1200 °C for 2 h (scan settings: 0.02°/ 1 s).

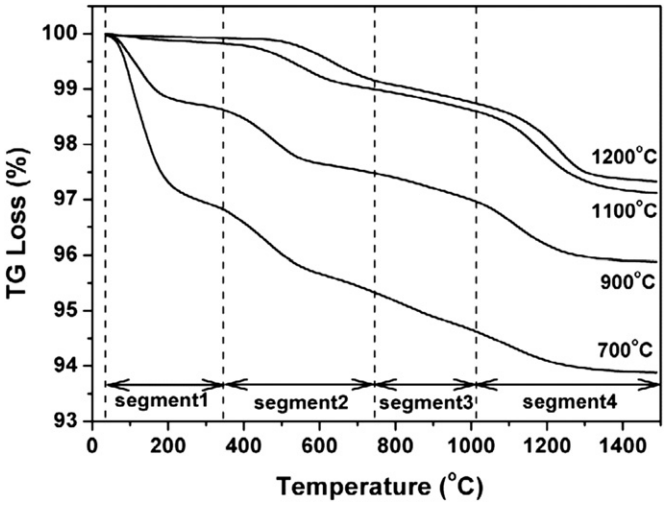

Fig. 2. TGA weight loss curves (under 5% CO/N_2 conditions) of C60Z samples calcined at various temperatures (dashed lines roughly divide the TGA weight loss curves into 4 segments).

toward lower angles. When the calcination temperature was above 1100 °C, a tiny peak adjacent to C60Z(111) ($2\theta = \sim 29°$), belonging to the Zr-rich phase, was observed, indicating that the phase separated into Ce-rich (cubic) and Zr-rich (tetragonal) phases [19,24–26].

Fig. 2 shows the TGA weight loss curves (under 5% CO/N_2 conditions) of C60Z samples calcined at 700–1200 °C for 2 h. The TGA weight loss can be divided into four segments. Segment 1 is attributed to the moisture or absorbed gas on the powder surface, which is related to the specific surface area of the samples. The TGA weight loss of segment 1 for the sample calcined at 700 °C for 2 h (3.09%) was about twice that for the sample calcined at 900 °C for 2 h (1.33%, Table 1), which is consistent with the variation of the BET value (Table 2). In addition, the TGA weight loss of the segment 1 was insignificant for the

Table 1
Reduction behavior of C60Z samples calcined at various temperatures.

Calcination temperature (°C)	Reduction behavior calculated from TGA/DTGA					
	Segment	Range (°C)	Peak position (°C)[a]	Reduction fraction (%)[b]	TGA weight loss in segments 2–4 (%)	TGA weight loss in segment 1 (%)
700	1	34–312	98	n/a		3.09
	2	312–592	461	40.52		
	3	592–902	n/a	26.32		
	4	902–1490	1101	33.16		
					3.13	
900	1	34–317	94	n/a		1.33
	2	317–606	477	36.76		
	3	606–968	n/a	20.73		
	4	968–1490	1117	42.51		
					2.84	
1100	1	34–368	n/a	n/a		0.19
	2	368–664	567	26.62		
	3	664–993	n/a	17.05		
	4	993–1490	1182	56.33		
					2.70	
1200	1	34–427	n/a	n/a		0.09
	2	427–806	646	32.87		
	3	806–1060	n/a	15.92		
	4	1060–1490	1247	51.21		
					2.58	

[a]The peak position is defined from the DTGA profiles.
[b]The fraction of TGA weight loss at each segment for segments 2–4.

Table 2
BET specific surface area and OSC measurement of C60Z samples calcined at various temperatures.

Calcination temperature (°C)	700	900	1100	1200
BET (m^2/g)	91.1	41.5	3.9	1.1
OSC (μmol/g)[a]	658	490	319	264

[a]The OSC was calculated by converting the sample to $Ce_{0.6}Zr_{0.4}O_2$ per gram.

samples with low surface areas (samples calcined at 1100 and 1200 °C for 2 h). The TGA weight loss from segments 2–4 for C60Z samples is attributed to the reduction reaction.

The TGA weight loss stages become more obvious after differentiation (differential thermogravimetric analysis, DTGA). The DTGA profiles are similar to temperature programmed reduction (TPR) curves in H_2 flow [1,9]. Fig. 3 shows the DTGA curves (under 5% CO/N_2 conditions) for C60Z samples calcined at various temperatures. For temperatures above 300 °C (excluding segment 1), the DTGA curves show two major reduction peaks for all C60Z samples. One appears in the low-temperature region (LT peak, segment 2) and the other is located in the high-temperature region (HT peak, segment 4). The DTGA curve in segment 3 is not obvious due to the TGA weight loss in segment 3 being too smooth to form a complete DTGA peak. For C60Z samples calcined at 700 and 900 °C (phases not separated yet) the LT and HT

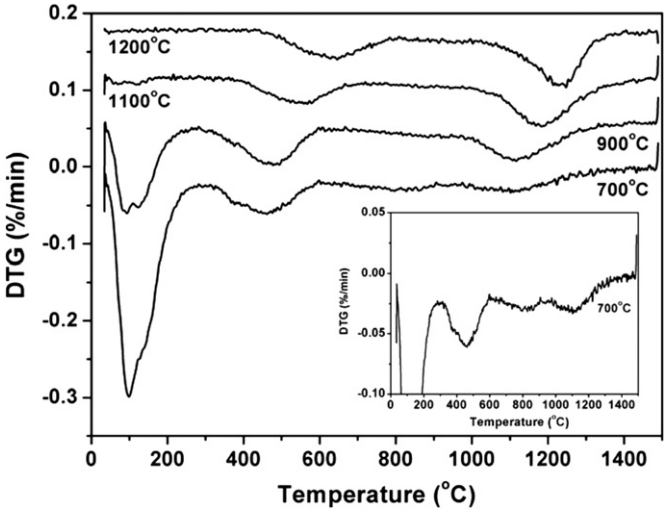

Fig. 3. DTGA curves (under 5% CO/N_2 conditions) of C60Z samples calcined at various temperatures. The inset shows the *y*-axis magnification of DTGA curve for the sample calcined at 700 °C for 2 h.

peaks are located at about 470 and 1110 °C, respectively. For C60Z samples calcined at 1100 and 1200 °C, the LT and HT peaks are located at 560–650 and 1180–1250 °C, respectively. The LT and HT peaks for the samples calcined at 1100 and 1200 °C are shifted about 100 °C higher compared to that for the samples calcined at 700 and 900 °C. These results indicate that the reduction temperature increased, and the reduction fraction decreased at the LT peak and increased at the HT peak

with increasing calcination temperature (Table 1). The above reduction behavior is in good agreement with observations reported by Trovarelli et al. [9] and Wang et al. [4].

The theoretical TGA weight loss for all Ce^{+4} ions reduced to Ce^{+3} ions in C60Z is 3.14%. The TGA weight loss for the samples calcined at 700 °C for 2 h was 3.13% (excluding segment 1, Table 1), which is very close to the theoretical value (it was assumed that the TGA weight loss of segments 2–4 is due to the loss of oxygen associated with the reduction of Ce^{+4} to Ce^{+3}) [4], indicating that almost all Ce^{+4} ions reduced to Ce^{+3} ions in C60Z. The TGA weight loss in segments 2–4 decreased with increasing calcination temperature, indicating that the reducibility of C60Z became worse with increasing calcination temperature.

The maximum OSC (658 μmol/g, Table 2) was obtained for the sample calcined at 700 °C for 2 h. The OSC degraded with increasing calcination temperature, which is consistent with the results of the reduction behavior (Fig. 3). Fig. 4 shows the TGA curves for C60Z samples after two redox cycles. The redox behaviors of the C60Z samples are almost the same for the first and the second redox cycles except for the sample calcined at 1200 °C for 2 h. The redox behavior in the second redox cycle for that sample severely degraded compared to that in the first redox cycle.

The BET specific surface area of the sample calcined at 900 °C (41.5 m^2/g) dropped about 50% compared to that of the sample calcined at 700 °C (91.1 m^2/g). However, the reduction temperature was almost the same and the reduction fraction of the LT peak was slightly decreased for the sample calcined at 900 °C (Table 1). Moreover, the OSC values also exhibited poor correlation to the BET values with increasing calcination temperature (Table 2). The above results indicate that another easier reduction species might occur concurrently besides the surface reduction at low temperature [14]. The phase separation of C60Z appeared after calcination at above 1100 °C for 2 h in air. The reduction temperature, fraction, and OSC of C60Z all significantly degraded after the appearance of phase separation. These results suggest that apart from the decreased surface area, the deterioration of reduction behavior and OSC might be attributed to the appearance of phase separation. The inhomogeneity caused by the phase separation might inhibit oxygen release in the CZ system [27].

Fig. 5((a)–(c)) shows the XRD patterns of C60Z samples calcined at 1100 °C for 2 h in air, heated to 1490 °C under a 5% CO/N_2 atmosphere, and then heated at 1200 °C for 2 h in air, respectively. Surprisingly, the separated phases obtained after calcination at 1100 °C for 2 h in air transformed into a pyrochlore structure (cation ordering) after heat treatment at 1490 °C under a 5% CO/N_2 atmosphere (Fig. 5(b)). Then, the pyrochlore transformed into three phases, namely C60Z (major phase) and Ce-rich and Zr-rich phases, after heat treatment at 1200 °C for 2 h in air (Fig. 5(c)), indicating phase separation appeared again. The transformation of pyrochlore into two phases was also observed by Otobe et al. [28] in the $Ce_{0.5}Zr_{0.5}O_2$ system. The color of C60Z samples was yellow after calcination in air and changed to gray black after heat treatment under a 5% CO/N_2 atmosphere, and then back to yellow again after heat treatment in air. Fig. 6((a)–(c)) shows the XRD patterns of C60Z calcined at 700 °C for 2 h in air, heated to 1490 °C under a 5% CO/N_2 atmosphere, and then heated at 1000 °C for 2 h in air, respectively. The single cubic phase for the sample calcined at 700 °C for 2 h transformed into a pyrochlore structure after heat treatment at 1490 °C under a 5% CO/N_2 atmosphere. It transformed back into a single cubic phase after further heat treatment at 1000 °C for 2 h in air. It should be noted that the two separated phases (Ce-rich and Zr-rich phases) transform into a pyrochlore structure after

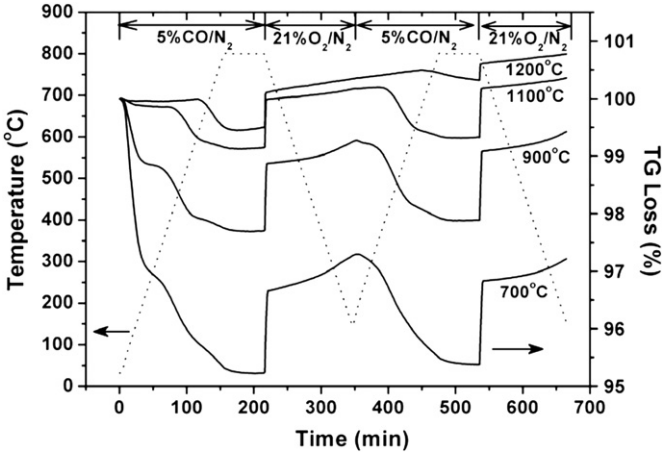

Fig. 4. TGA curves of C60Z samples calcined at various temperatures under reduction/re-oxidation conditions for two cycles.

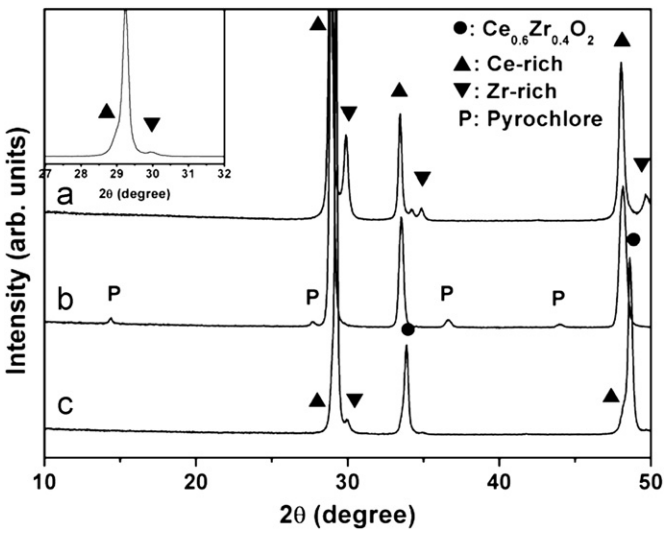

Fig. 5. XRD patterns of C60Z samples (a) calcined at 1100 °C for 2 h in air, (b) heated to 1490 °C under a 5% CO/N_2 atmosphere, and then (c) heated at 1200 °C for 2 h in air. The inset shows the local magnification of (c) (scan settings: 0.02°/8 s).

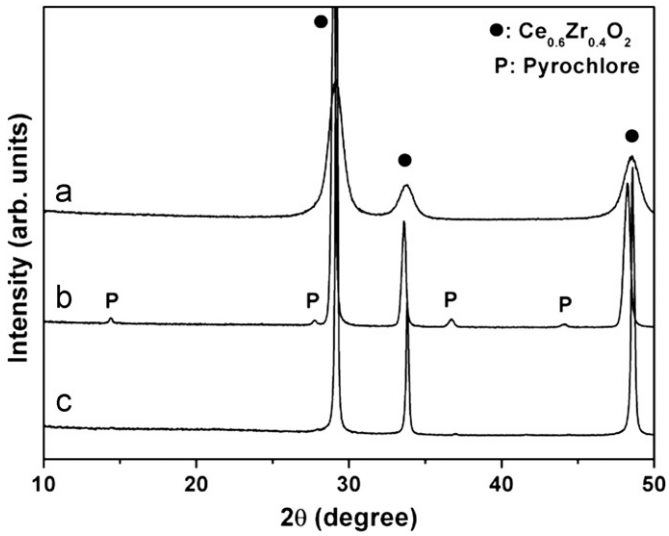

Fig. 6. XRD patterns of C60Z samples (a) calcined at 700 °C for 2 h in air, (b) heated to 1490 °C under a 5% CO/N_2 atmosphere, and (c) heated at 1000 °C for 2 h in air again (scan settings: 0.02°/8 s).

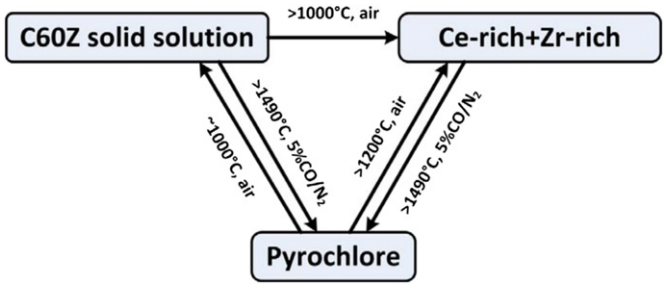

Fig. 7. Schematic diagram for phase transformation of C60Z under reduction/re-oxidation treatment.

heat treatment at high temperature under a reducing atmosphere, and then this structure transforms back into the phase separation state after further heat treatment in air, suggesting that the phase transformation (disorder–order transition) under reduction/re-oxidation treatment might be attributed to cation diffusion. Fig. 7 shows a phase transformation schematic diagram of C60Z under reduction/re-oxidation treatment.

4. Conclusion

The relationship between the crystalline structure and reduction behavior of C60Z synthesized using the chemical co-precipitation method was investigated. C60Z decomposes from a single cubic phase into Ce-rich (cubic) and Zr-rich (tetragonal) phases after calcination at above 1100 °C. The weight loss from the reduction reaction under a 5% CO/N_2 atmosphere for the sample calcined at 700 °C for 2 h was 3.13% (TGA weight loss of segments 2–4), which is very close to the theoretical calculation for all Ce^{4+} ions reduced to Ce^{3+} ions (3.14%). The reduction peak and the reduction fraction were shifted to higher temperatures after the appearance of phase separation for C60Z samples. The optimal OSC (658 μmol/g) was obtained for the sample calcined at 700° C for 2 h. The OSC then decreased with increasing calcination temperature. The reducibility and OSC property decreased after the appearance of phase separation. The inhomogeneity originating from the phase separation may inhibit the oxygen release in the CZ system.

The two separated phases (Ce-rich and Zr-rich phases) obtained after calcination at 1100 °C for 2 h transformed into a pyrochlore structure after heat treatment under a reducing atmosphere (5% CO/N_2), and then this structure transformed into separated phases after further treatment in air, suggesting that the phase transformation (disorder–order transition) under reduction/re-oxidation treatment might be attributed to cation diffusion.

Acknowledgment

This work was supported by the Ministry of Economic Affairs (100-EC-17-A-08-S1-170) through the Particulate Materials Research Center of National Cheng Kung University.

References

[1] P. Fornasiero, R. Di Monte, G.R. Rao, J. Kaspar, S. Meriani, A. Trovarelli, M. Graziani, Rh-loaded CeO_2–ZrO_2 solid-solutions as highly efficient oxygen exchangers: dependence of the reduction behavior and the oxygen storage capacity on the structural properties, Journal of Catalysis 151 (1995) 168–177.

[2] S. Ricote, G. Jacobs, M. Milling, Y. Ji, P.M. Patterson, B.H. Davis, Low temperature water-gas shift: characterization and testing of binary mixed oxides of ceria and zirconia promoted with Pt, Applied Catalysis A: General 303 (2006) 35–47.

[3] E. Mamontov, T. Egami, R. Brezny, M. Koranne, S. Tyagi, Lattice defects and oxygen storage capacity of nanocrystalline ceria and ceria–zirconia, Journal of Physical Chemistry B 104 (2000) 11110–11116.

[4] R.G. Wang, P.A. Crozier, R. Sharma, J.B. Adams, Nanoscale heterogeneity in ceria–zirconia with low-temperature redox properties, Journal of Physical Chemistry B 110 (2006) 18278–18285.

[5] S. Damyanova, B. Pawelec, K. Arishtirova, M.V.M. Huerta, J.L.G. Fierro, Study of the surface and redox properties of ceria–zirconia oxides, Applied Catalysis A: General 337 (2008) 86–96.

[6] H. Vidal, J. Kaspar, M. Pijolat, G. Colon, S. Bernal, A. Cordon, V. Perrichon, F. Fally, Redox behavior of CeO_2–ZrO_2 mixed oxides: II. influence of redox treatments on low surface area catalysts, Applied Catalysis B: Environmental 30 (2001) 75–85.

[7] T. Omata, H. Kishimoto, S. Otsuka-Yao-Matsuo, N. Ohtori, N. Umesaki, Vibrational spectroscopic and X-ray diffraction studies of cerium–zirconium oxides with Ce/Zr composition ratio=1 prepared by reduction and successive oxidation of t'-$(Ce_{0.5}Zr_{0.5})O_2$ phase, Journal of Solid State Chemistry 147 (1999) 573–583.

[8] G. Balducci, J. Kaspar, P. Fornasiero, M. Graziani, M.S. Islam, J.D. Gale, Computer simulation studies of bulk reduction and oxygen migration in CeO_2–ZrO_2 solid solutions, Journal of Physical Chemistry B 101 (1997) 1750–1753.

[9] A. Trovarelli, F. Zamar, J. Llorca, C. de Leitenburg, G. Dolcetti, J.T. Kiss, Nanophase fluorite-structured CeO_2–ZrO_2 catalysts prepared by high-energy mechanical milling, Journal of Catalysis 169 (1997) 490–502.

[10] A. Gupta, U.V. Waghmare, M.S. Hegde, Correlation of oxygen storage capacity and structural distortion in transition-metal-, noble-metal-, and rare-earth-ion-substituted CeO_2 from first principles calculation, Chemistry of Materials 22 (2010) 5184–5198.
[11] Z. Yang, T.K. Woo, K. Hermansson, Effects of Zr doping on stoichiometric and reduced ceria: a first-principles study, Journal of Chemical Physics 124 (2006) 224704–224710.
[12] Y. Madier, C. Descorme, A.M. Le Govic, D. Duprez, Oxygen mobility in CeO_2 and $Ce_xZr_{(1-x)}O_2$ compounds: study by CO transient oxidation and $^{18}O/^{16}O$ isotopic exchange, Journal of Physical Chemistry B 103 (1999) 10999–11006.
[13] A.S. Ivanova, Physicochemical and catalytic properties of system based on CeO_2, Kinetics and Catalysis 50 (2009) 797–815.
[14] L. Meng, L. Liu, X. Zi, H. Dai, Z. Zhao, X. Wang, H. He, Preparation of ceria–zirconia solid solution with enhanced oxygen storage capacity and redox performance, Frontiers of Environmental Science and Engineering in China 4 (2010) 164–171.
[15] H.C. Yao, Y.F.Y. Yao, Ceria in automotive exhaust ctalysts, Journal of Catalysis 86 (1984) 254–265.
[16] P. Fornasiero, G. Balducci, R. Di Monte, J. Kaspar, V. Sergo, G. Gubitosa, A. Ferrero, M. Graziani, Modification of the redox behaviour of CeO_2 induced by structural doping with ZrO_2, Journal of Catalysis 164 (1996) 173–183.
[17] H. Vidal, J. Kaspar, M. Pijolat, G. Colon, S. Bernal, A. Cordon, V. Perrichon, F. Fally, Redox behavior of CeO_2–ZrO_2 mixed oxides: I. influence of redox treatments on high surface area catalysts, Applied Catalysis B: Environmental 27 (2000) 49–63.
[18] R. Di Monte, J. Kaspar, On the role of oxygen storage in three-way catalysis, Topics in Catalysis 28 (2004) 47–57.
[19] R. Di Monte, J. Kaspar, Nanostructured CeO_2–ZrO_2 mixed oxides, Journal of Materials Chemistry 15 (2005) 633–648.
[20] N. Izu, T. Omata, S. Otsuka-Yao-Matsuo, Oxygen release behaviour of $Ce_{(1-x)}Zr_xO_2$ powders and appearance of $Ce_{(8-4y)}Zr_{4y}O_{(14-\delta)}$ solid solution in the ZrO_2–CeO_2–$CeO_{1.5}$ system, Journal of Alloys and Compounds 270 (1998) 107–114.
[21] N. Izu, H. Kishimoto, T. Omata, K. Ono, S. Otsuka-Yao-Matsuo, oxygen release behavior of metastable tetragonal t'_{meta}-$(Ce_{0.5}Zr_{0.5})O_2$ phases prepared by reduction and successive oxidation of t' phase, Science and Technology of Advanced Materials 2 (2001) 397–404.
[22] S. Otsuka-Yao-Matsuo, H. Morikawa, N. Izu, K. Okuda, oxygen evolution properties of CeO_2–ZrO_2 powders as automotive exhaust sub-catalysts and the phase diagrams, Journal of the Japan Institute of Metals 59 (1995) 1237–1246.
[23] S. Otsuka-Yao-Matsuo, T. Omata, N. Izu, H. Kishimoto, Oxygen release behavior of $CeZrO_4$ powders and appearance of new compounds κ and t*, Journal of Solid State Chemistry 138 (1998) 47–54.
[24] K. Kenevey, F. Valdivieso, M. Soustelle, M. Pijolat, Thermal stability of Pd or Pt loaded $Ce_{0.68}Zr_{0.32}O_2$ and $Ce_{0.50}Zr_{0.50}O_2$ catalyst materials under oxidising conditions, Applied Catalysis B: Environmental 29 (2001) 93–101.
[25] G. Colon, F. Valdivieso, M. Pijolat, R.T. Baker, J.J. Calvino, S. Bernal, Textural and phase stability of $Ce_xZr_{1-x}O_2$ mixed oxides under high temperature oxidising conditions, Catalysis Today 50 (1999) 271–284.
[26] H.-W. Jen, G.W. Graham, W. Chun, R.W. McCabe, J.-P. Cuif, S.E. Deutsch, O. Touret, Characterization of model automotive exhaust catalysts: Pd on ceria and ceria–zirconia supports, Catalysis Today 50 (1999) 309–328.
[27] Y. Nagai, T. Yamamoto, T. Tanaka, S. Yoshida, T. Nonaka, T. Okamoto, A. Suda, M. Sugiura, Local structure analyses of $Ce_{0.5}Zr_{0.5}O_2$ mixed oxides by XAFS, Journal of Synchrotron Radiation 8 (2001) 616–618.
[28] H. Otobe, A. Nakamura, T. Yamashita, K. Minato, Oxygen potential and defect structure of oxygen-excess pyrochlore $Ce_2Zr_2O_{7+x}$, Journal of Physics and Chemistry of Solids 66 (2005) 329–334.